Available online at www.sciencedirect.com
SCIENCE DIRECT®
International Journal of Thermal Sciences 42 (2003) 813–820
International Journal of Thermal Sciences
www.elsevier.com/locate/ijts

Green element procedures for transport accompanied by nonlinear reaction

Okey Oseloka Onyejekwe

New England College, 7 Main Street, Henniker, NH 03242-2397, USA

Received 9 November 2001; accepted 30 August 2002

Abstract

Certain key characteristics of a general transport process accompanied by a mathematical non-linearity of the governing equation due to the chemical reaction term are studied with a hybrid boundary integral technique known as the Green element method (GEM). The weighting function employed is the singular solution of the one-dimensional Laplace equation, and the non-linearity is resolved by the standard Newton–Raphson and Picard methods. A number of illustrative problems are solved using this algorithm, and in each case, it is simply demonstrated that GEM is both reliable and adequate for the accurate prediction of field variables.

Keywords: Non-linearity; Boundary integral technique; Green element method

1. Introduction

Mass transport of species accompanied by chemical reaction has a ubiquitous presence in several areas of medicine, engineering and science. For example in combustion and flame propagation, in contamination and remediation of aqueous environments, arterial blood circulation, design of heterogeneous reactors, and various enzymatic and biochemical reactions to mention just a few. Fundamentally the study of nonlinear reaction kinetics and diffusion paves the way for a thorough understanding of these physical processes. Sometimes the time scales of diffusion and reaction processes can vary significantly. This introduces steep profiles of dependent variables during solution, as is the case with combustion where mass transport of species is often accompanied by a rapid reaction within an active zone. The development of a general mathematical model describing several aspects of interaction between chemical, thermal and mass transfer processes is therefore very challenging. Some early attempts to deal with these types of problems can be found in Lavoie et al. [1], Blumberg [2], Mills et al. [3], Patridge and Wrobel [4], and Ramachandran [5].

Of the various methods mentioned in literature, the application has generally progressed in two directions involving (i) the domain based methods, i.e., finite difference and finite element techniques, and (ii) the boundary based method, for example, the boundary integral methods. The integral formulation based on the boundary integral method is a well-established numerical procedure for solving engineering problems. An essential feature of the technique is the conversion of the governing partial differential equation into its integral equivalent by the use the Green's second identity equation. The solution of an adjoint differential equation is then used as the weighting function for the *weak integral formulation*. In most cases, the boundary integral equations are only satisfied at discrete number of points resulting in unsymmetric matrices of the systems of linear algebraic equations. In addition *boundary only* implementation of standard BEM makes the global matrices *fully populated*. A concomitant problem therefore is the difficulty encountered in handling unsymmetric and fully populated matrices efficiently, especially for large-scale problems. A multi-zone approach has often been adopted as a way of creating an overall system of equations that could be better handled numerically (Lafe et al. [6]). By hindsight, this could be said to be one of the initial attempts by boundary-element practitioners to effectively deal with the problem domain. (Lafe and Cheng [7]) introduced a *perturbation technique* as a way of handling media heterogeneity. The method however failed to yield accurate result when applied to rapid variations of hydraulic conductivity in the problem domain.

E-mail address: okuzaks@yahoo.com (O.O. Onyejekwe).

1290-0729/03/$ – see front matter
doi:10.1016/S1290-0729(03)00036-X

Nomenclature

A	constant term in boundary conditions
B	constant term in boundary conditions
D	dimensionless diffusion coefficient
g_i	left-hand side of nonlinear algebraic equation
e	iteration parameter
J_{ij}	Jacobian matrix
κ	longest element length
L_{ij}	equation matrix coefficient
p	equation parameter that defines geometry
q	problem constant that defines boundary condition
T_{ij}, S_{ij}, R_{ij}, P_{ijk}	equation coefficient matrices
x	space coordinate
x_i	x coordinate linked to nodal position (source point)
α_z	time scheme weighting factor
Δ	small increment
λ	contact coefficient
$\varphi(x,t)$	dimensionless mass concentration
$\varphi^0(x,0)$	initial mass concentration
$\psi(x,t)$	spatial derivative of mass concentration
Ω_j	linear basis function

Subscripts

(k, j, i)	rows and columns of matrix equation

Superscripts

$m, m+1$	previous and current time levels
$e, e+1$	previous and current iterations

Experiences like these place BEM at a disadvantage when domain integrals are encountered. For example when BEM is applied to nonlinear, heterogeneous and time dependent problems involving sources and sinks, its *boundary only* formulation is invariably lost or seriously compromised. Efforts to restore this have resulted in numerical schemes like the dual reciprocity method (DRM) by Nardini and Brebbia [8], and the particular integrals technique (PIT) by Ahmad and Barnerjee [9]. Apart from an extra numerical rigor involved in converting domain integrals into equivalent boundary integrals, such schemes are still plagued by fully populated matrices. In addition they have been found to be restricted to problems restricted to weak nonlinearities or small *Peclet numbers*. (Popov and powers [10], Archer et al. [11].)

In the light of all these numerical difficulties severely restricting the ability of BEM to tackle large scale or realistic engineering problems, there now seems to be a consensus of opinion among a good number of BEM enthusiasts that the way forward is to incorporate within BEM formulation, an efficient technique for dealing with domain integrals. This idea has been approached from two fundamentally different points. While a particular approach still strives to maintain BEMs *boundary only* character even when dealing with domain sources the others adopt a *hybrid approach* which introduces the robustness of other domain based methods especially finite element technique into BEMs. The Green element method (GEM), (Taigbenu [12], Taigbenu [13], Onyejekwe [14], Onyejekwe [15], Onyejekwe [16]) falls within the second category. GEM overcomes the problems associated with the boundary element method by adopting the FEM-type domain mesh and solving the integral equations of BEM on each element, after continuity conditions are imposed on element interfaces.

On the other hand, the recently formulated DRM-MD approach (Popov and Powers [10]) still adopts domain—decomposition, but unlike GEM, the domain integrals are converted into surface integrals at the contour of each sub region by the dual reciprocity method (DRM) using radial basis functions. In principle, the DRM-MD method is essentially similar to GEM except that no cell integration is performed on each element.

This paper utilizes the hybrid boundary integral procedure known as GEM to solve nonlinear equations of complex kinetic reaction processes in a slab, cylinder and a sphere as well as a flame propagation problem, which displays some features of combustion. For most parts, the accuracy of the solution is established on the basis of comparison with the results of identical problems available in literature.

2. Model problems

2.1. Coupled nonlinear combustion

The first model presented herein is that of Otey and Dwyer [17]. It comprises the two coupled diffusion–reaction equations:

$$\frac{\partial \overline{\rho}}{\partial \overline{t}} = \alpha_D \frac{\partial^2 \overline{\rho}}{\partial \overline{X^2}} - K_1 \overline{\rho} \tag{1a}$$

$$\rho_0 C_p \frac{\partial \overline{T}}{\partial \overline{t}} = k \frac{\partial^2 \overline{T}}{\partial \overline{X^2}} + \Delta h_0 K_1 \overline{\rho} \tag{1b}$$

where $\overline{\rho}$ is the material density, $\overline{X}, t$ are the independent space and time variables, α_D, k are diffusion coefficient and thermal conductivity, respectively, $\overline{T}$ is the temperature, Δh_0 represents the heat of reaction, C_p is the specific heat at constant pressure and K_1 is the reaction rate constant. For the sake of brevity, the bar sign will no longer be

considered on any of the variables. The above coupled nonlinear equations represent a simplified form of the energy equation with a chemical reaction source term in which the following assumptions have been made namely:

(a) constant physical properties;
(b) no convection;
(c) one-dimensional continuum;
(d) no external heat source.

The one-dimensional assumption, though a key assumption does not eliminate the major features of the combustion process apart from simplifying the governing equations.

Before embarking on the mathematical treatment of this model, we shall dwell briefly on some of the key features, which it represents. The process under consideration results from interactions of species diffusion, heat conduction and chemical reaction. The form of the coordinate shows that we shall limit our attention to a planar geometry. Attention will be focused on nonlinearities introduced by chemical reactions as well as diffusion and conduction of state variables. The reaction rate constant is an exponential function of temperature describing the Arrhenius type reaction:

$$K_1 = K_0 \mathrm{e}^{-E/RT} \tag{2}$$

where R is the universal gas constant, and E is the Arrhenius activation energy. Making use of the constant physical property assumption equation (1a) and (1b) can be nondimensionalized using the method adopted by Otey and Dwyer [17]. We finally obtain:

$$\frac{\alpha}{\alpha_D}\frac{\partial \rho}{\partial t} = \frac{\partial^2 \rho}{\partial X^2} - \frac{L^2 K_1}{\alpha_D}\rho \tag{3a}$$

$$\frac{\partial T}{\partial t} = \frac{\partial^2 T}{\partial X^2} + \frac{L^2 K_1}{\alpha_D}\rho \tag{3b}$$

where L is the length of the problem domain, and $L^2 K_1 \rho/\alpha_D$ is the Damköhler's number. We introduce another constant: $A = K_0 L^2/\alpha$. The ratio of thermal and mass diffusivities α/α_D is assumed equal. Eqs. (3a) and (3b) can now be represented by:

$$\frac{\partial \rho}{\partial t} = \frac{\partial^2 \rho}{\partial X^2} - A\rho \mathrm{e}^{-\theta/T} \tag{4a}$$

$$\frac{\partial T}{\partial t} = \frac{\partial^2 T}{\partial X^2} + A\rho \mathrm{e}^{-\theta/T} \tag{4b}$$

where A is a dimensionless rate constant, and θ is dimensionless activation energy. The initial and boundary conditions for the solution of Eqs. (4a) and (4b) are the same as those given by Otey and Dwyer [17]. For a typical temperature ratio of six, occurring in a hydrocarbon fuel burning in air, the initial and final dimensionless mass and temperature gradients a swell as temperature are specified as:

$$\frac{\partial \rho}{\partial X} = 0.0, \qquad \frac{\partial T}{\partial X} = 0.0 \quad \text{at } X = 0$$

$$\frac{\partial \rho}{\partial X} = 0.0, \qquad T = T_i + C_1 t \quad \left(t < \frac{1}{C_1}\right)$$

$$T = T_f \quad \left(t \succ \frac{1}{C_1}\right) \quad \text{at } X = 1 \tag{5}$$

where C_1 is a constant. $C_1 = 0.002$, $\theta = 4.0$. The exponential terms in the coupled nonlinear equations indicate a sensitive ignition process. It has been suggested that the time it takes for the chemical reaction to deviate from the temperature of the conduction solution serves as the initial time for starting flame propagation prediction (Raizadeh [18]). The boundary and initial conditions so specified are designed to enhance the simplicity of the analysis while at the same time retain the qualitative features of the model problem. Here, we consider the conversion so species A to species B, $A \Rightarrow B$ in a process governed by the one-dimensional coupled nonlinear differential equation. Since the system defies an analytical method of solution, we choose to employ GEM numerical technique to determine the scalar profiles as well as other problem parameters of interest.

2.2. Transport of a reactant in a reactor

For the second problem, we consider a partial differential equation describing the concentration profile of a reactant along a reactor:

$$\frac{\partial \varphi}{\partial t} = \frac{1}{x^p}\frac{\partial}{\partial x}\left(Dx^p \frac{\partial \varphi}{\partial x}\right) + \frac{M\varphi}{1 + c\varphi + \beta\varphi^2} \tag{6}$$

where φ is the mass concentration, x is the space independent variable, where M is the Thiele modulus, c and β are problem constants, and the parameter values $p = 0, 1, 2$ are used to convert Eq. (6) to that of a slab, cylinder or sphere, respectively. The nonnegative constant D represents the diffusion coefficient, and the nonlinear reaction term describes the kinetics of the medium. The initial and boundary conditions can generally be put in the form:

$$\varphi(x, 0) = \varphi^0(x) \tag{7a}$$

$$Q\frac{\partial \varphi}{\partial x} + B\varphi = V \tag{7b}$$

where Q, B, V are constants whose values depend on whether the boundary conditions are Dirichlet, Neumann or Cauchy.

3. Green element discretization

The conversion of the governing partial differential equations (4a), (4b) and (6) to integro-differential forms is achieved by utilizing the *Green's second identity* and an *auxiliary differential equation* $\frac{\mathrm{d}^2 G}{\mathrm{d}x^2} = \delta(x - x_i)$ and its solution $G(x, x_i) = 0.5[|x - x_i| + \kappa]$ where κ is an arbitrary constant, and is represented by the length of the longest element in the problem domain. Details of the computation steps involved in this conversion are clearly ex-

plained in earlier works (Onyejekwe [13]). Within a typical linear element $\lfloor x_1, x_2 \rfloor$, the resulting integro-diferntial forms representing slab, cylindrical and spherical geometries as well as nonlinear coupled equations are given as:

For a slab:

$$\begin{aligned}&\big[-\lambda\varphi(x_i,t)+G^*(x_2,x_i)\varphi(x_2,t)-G^*(x_1,t)\varphi(x_1,t)\\&\quad-G(x_2,x_i)\psi(x_2,t)+G(x_1,x_i)\psi(x_1,t)\big]\\&\quad+\int_{x_1}^{x_2}\frac{G}{D}\left[\frac{\partial\varphi}{\partial t}+f(\varphi)\right]\mathrm{d}x=0\end{aligned}\tag{8a}$$

where

$$f(\varphi)=\frac{M\varphi}{1+c\varphi+\beta\varphi^2}$$

For cylinder:

$$\begin{aligned}&\big[-\lambda\varphi(x_i,t)+G^*(x_2,x_i)\varphi(x_2,t)-G^*(x_1,t)\varphi(x_1,t)\\&\quad-G(x_2,x_i)\psi(x_2,t)+G(x_1,x_i)\psi(x_1,t)\big]\\&\quad+\int_{x_1}^{x_2}G(x,x_i)\left[\frac{1}{D}\frac{\partial\varphi}{\partial t}+f(\varphi)-\frac{p}{x}\frac{\partial\varphi}{\partial x}\right]\mathrm{d}x=0\end{aligned}\tag{8b}$$

For the nonlinear coupled equations:

$$\begin{aligned}&\big[-\lambda\rho(x_i,t)+G^*(x_2,x_i)\rho(x_2,t)-G^*(x_1,t)\rho(x_1,t)\\&\quad-G(x_2,x_i)\nu(x_2,t)+G(x_1,x_i)\nu(x_1,t)\big]\\&\quad+\int_{x_1}^{x_2}G(x,x_i)\left[\frac{\partial\rho}{\partial t}+A\rho\mathrm{e}^{-\theta/T}\right]\mathrm{d}x=0\end{aligned}\tag{8c}$$

$$\begin{aligned}&\big[-\lambda T(x_i,t)+G^*(x_2,x_i)T(x_2,t)-G^*(x_1,t)T(x_1,t)\\&\quad-G(x_2,x_i)\Theta(x_2,t)+G(x_1,x_i)\Theta(x_1,t)\big]\\&\quad+\int_{x_1}^{x_2}G(x,x_i)\left[\frac{\partial T}{\partial t}-A\rho\mathrm{e}^{-\theta/T}\right]\mathrm{d}x=0\end{aligned}\tag{8d}$$

where λ is the contact coefficient, $\nu(X,t)=\frac{\partial\rho}{\partial X}$, $\Theta(X,t)=\frac{\partial T}{\partial X}$, $Q\frac{\partial\varphi}{\partial x}+B\varphi=V$. The following systems of discrete equations are obtained for Eqs. (8a), (8b), (8c) and (8d), respectively:

For a slab:

$$R_{ij}\varphi_j+L_{ij}\psi_j+N_{ij}\left(\frac{\mathrm{d}\varphi_j}{\mathrm{d}t}+f(\varphi)_j\right)\tag{9a}$$

For a cylinder:

$$R_{ij}\varphi_j+\big(L_{ij}-S_{ij}^p\big)\psi_j+N_{ij}\left(\frac{\mathrm{d}\varphi_j}{\mathrm{d}t}+f(\varphi)_j\right)=0\tag{9b}$$

For the nonlinear coupled equations:

$$R_{ij}\rho_j+L_{ij}\nu_j+P_{ijk}\left[\frac{\mathrm{d}\rho_j}{\mathrm{d}t}+A\rho\mathrm{e}^{-\theta/T_k}\right]=0\tag{9c}$$

$$R_{ij}T_j+L_{ij}\Theta_j+P_{ijk}\left[\frac{\mathrm{d}\rho_j}{\mathrm{d}t}-A\rho\mathrm{e}^{-\theta/T_k}\right]=0\tag{9d}$$

The element matrices for a slab are given elsewhere (Onyejekwe [14], Onyejekwe [15]), those related to the cylindrical coordinates are put in the form:

$$S_{ij}^1=\int_{x_1}^{x_2}\left[\frac{\Omega_j}{x}\right]G(x,x_i)\,\mathrm{d}x\tag{10}$$

where Ω_j are element interpolation functions. A generalized 2-level time discretization scheme is employed for the time derivatives. This results in the following equations:

For a slab:

$$\begin{aligned}&\alpha_z\big(DR_{ij}\varphi_j^{(m+1)}+DL_{ij}\psi_j^{(m+1)}\big)\\&\quad+(1-\alpha_z)\big(DR_{ij}\varphi_j^{(m)}+DL_{ij}\psi_j^{(m)}\big)\\&\quad+N_{ij}\left[\frac{1}{\Delta t}\big(\varphi_j^{(m+1)}-\varphi_j^{(m)}\big)+(\alpha_z)\big(f(\varphi)_j^{(m+1)}\big)\right.\\&\qquad\left.+(1-\alpha_z)\big(f(\varphi)_j^{m}\big)\right]\equiv g_i=0\end{aligned}\tag{11a}$$

For a cylinder:

$$\begin{aligned}&\alpha_z\big(R_{ij}\varphi_j^{(m+1)}+D\big(L_{ij}-S_{ij}^p\big)\psi_j^{(m+1)}\big)\\&\quad+(1-\alpha_z)\big(DR_{ij}\varphi_j^{(m)}+D\big(L_{ij}-S_{ij}^p\big)\psi_j^{(m)}\big)\\&\quad+N_{ij}\left[\frac{1}{D\Delta t}\big(\varphi_j^{(m+1)}-\varphi_j^{(m)}\big)+(\alpha_z)\big(f(\varphi)_j^{(m+1)}\big)\right.\\&\qquad\left.+(1-\alpha_z)\big(f(\varphi)_j^{(m)}\big)\right]\equiv g_i=0\end{aligned}\tag{11b}$$

For the coupled nonlinear equation:

$$\begin{aligned}&\left[\alpha_z R_{ij}+\frac{P_{ijk}}{\Delta t}\right]\rho_j^{(m+1)}+(1-\alpha_z)\big[L_{ij}\big]\nu_j^{(m+1)}-\frac{P_{ijk}}{\Delta t}\rho_j\\&\quad+(1-\alpha_z)[L_{ij}]\nu_j^{(m)}\\&\quad-P_{ijk}\big[\alpha_z A\rho_j^{(m+1)}\mathrm{e}^{-\theta/T_k}\\&\qquad+(1-\alpha_z)A\rho_j^{(m)}\mathrm{e}^{-\theta/T_k}\big]\equiv g_i=0\end{aligned}\tag{11c}$$

$$\begin{aligned}&\left[\alpha_z R_{ij}+\frac{P_{ijk}}{\Delta t}\right]T_k^{(m+1)}+\alpha_z[L_{ij}]\Theta_j^{(m+1)}-\frac{P_{ijk}}{\Delta t}T_k^{(m)}\\&\quad+(1-\alpha_z)[L_{ij}]\Theta^{(m)}\\&\quad-P_{ijk}\big[\alpha_z A\rho_j^{(m+1)}\mathrm{e}^{-\theta/T_k^{(m+1)}}\\&\qquad+(1-\alpha_z)A\rho_j^{(m)}\mathrm{e}^{-\theta/T_k^{(m)}}\big]\equiv g_i=0\end{aligned}\tag{11d}$$

where the superscripts m and $m+1$ denote the previous and current time levels respectively, Δt is the time step, and α_z is a finite difference weighting factor. For all computations reported herein, α_z is assigned a value of 0.67, which in finite difference appellation is known the Galerkin scheme. The linearization of the algebraic equation is achieved by the implementation of the Newton–Raphson's algorithm. We adopt the following relationship for an estimate of the dependent variable $\xi^{(m+1,e)}$.

$$\xi^{(m+1,e+1)}=\xi^{(m+1,e)}+\Delta\xi^{(m+1,e+1)}\tag{12a}$$

where $\Delta\xi^{(m+1,e+1)}$ is the refinement of the initial estimate, and $e, e+1$ are the previous and current iteration levels. Folowing the Newton–Raphson algorithm,

$$J_{ij}^{(m+1,e)}\Delta\xi_j^{(m+1,e+1)} = -g^{(e)} \tag{12b}$$

where g_i is a vector of the discrete equations' left-hand sides evaluated at the previous iteration level, and $J_{ij}^{(m+1,e)}$ is the Jacobian matrix.

$$J_{ij}^{(m+1,e)}\begin{bmatrix}\Delta\varphi^{(m+1,e+1)}\\ \Delta\psi^{(m+1,e+1)}\end{bmatrix} = -g_i^{(m+1,e)} \tag{12c}$$

Without any loss in generality, the Jacobians for the cylindrical geometry is given by:

$$\begin{aligned} J_{ij}^{(m+1,e)} &= \left.\frac{\partial g_j}{\partial\varphi}\right|_{\varphi_j=\varphi_j^{(m+1,e)}} \\ &= \alpha_z R_{ij} + \alpha_z\mu T_{ij}2\varphi_j^{(m+1)} + \frac{\alpha_z N_{ij}}{D\Delta t} \end{aligned} \tag{12d}$$

We carry out the same procedure for the coupled equation to yield:

$$\left.\frac{\partial g_i}{\partial\rho_j}\right|_{\rho_j=\rho_j^{(m+1,e)}} = \alpha_z R_{ij} + \frac{P_{ijk}}{\Delta t} + P_{ijk}A\mathrm{e}^{-\theta/T_k}$$

$$\left.\frac{\partial g_i}{\partial v_j}\right|_{v_j=v_j^{(m+1,e))}} = \alpha_z L_{ij} \tag{12e}$$

$$\left.\frac{\partial g_i}{\partial T_j}\right|_{T_k=T_k^{(m+1,e)}} = \alpha_z R_{ij} + \frac{P_{ijk}}{\Delta t} - P_{ijk}A\rho_j\mathrm{e}^{-\theta/T_k}\frac{\theta}{T_k^2}$$

$$\left.\frac{\partial g_i}{\partial\psi_j}\right|_{\psi_j=\psi_j^{(m+1,e)}} = \alpha_z L_{ij} \tag{12f}$$

Another linearization technique, the Picard method is linearly convergent and has a simpler formulation than the Newton–Rahpson's method. For system of equations, GEM implementation of the Picard's algorithm yields:

$$Z_{ij}^{(e)}h_j^{(e+1)} = s_i\left(h_j^{(e)}\right) \tag{13a}$$

where e is the iteration number, $Z_{ij}^{(e)}$ is a pre-multiplying matrix, and is made up of elements, which depend solely on the previous iteration of the solution vector $h^{(e)}$ and $s_i(h^{(e)})$ is a known vector. Eq. (13a) can now be put in a more convenient form for computation:

$$h_j^{(e+1)} = \left[A_{ij}^{(e)}\right]^{-1}S_i\left\{h_j^{(e)}\right\} \tag{13b}$$

The Picard scheme is applied to Eqs. (11a) and (11b) to obtain:

$$\begin{aligned} &\left[R_{ij} + \left(\frac{\alpha_z}{\Delta t} + f(\varphi)_j^{m+1,e}\right)N_{ij}\right]\varphi_j^{m+1,e+1} \\ &\quad + (DL_{ij})\psi_j^{m+1,e+1} \\ &= N_{ij}\left[\frac{\alpha_z}{\Delta t}\varphi_j^m - (1-\alpha_z)\frac{\mathrm{d}\varphi_j^m}{\mathrm{d}t}\right. \\ &\qquad \left. - (1-\alpha_z)f(\varphi)_j^{m+1,e}\right] = 0 \end{aligned} \tag{13c}$$

$$\begin{aligned} &\left[R_{ij} + \left(\frac{\alpha_z}{\Delta t} + f(\varphi)_j^{m+1,e}\right)N_{ij}\right]\varphi_j^{m+1,e+1} \\ &\quad + D\left(L_{ij} - S_{ij}^p\right)\psi_j^{m+1,e+1} \\ &= N_{ij}\left[\frac{\alpha_z}{\Delta t}\varphi_j^m - (1-\alpha_z)\frac{\mathrm{d}\varphi_j^m}{\mathrm{d}t}\right. \\ &\qquad \left. - (1-\alpha_z)f(\varphi)_j^{m+1,e}\right] = 0 \end{aligned} \tag{13d}$$

The Newton–Raphson and the Picard's schemes are denoted as *model-1* and *model-2*, respectively. The finite-difference solutions of Otey and Dwyer [17] incorporating the Newton–Raphson linearization are used as our basis for comparison. This is referred to as *model-3*.

4. Presentations and discussion of results

Example 1. For the validation of the method presented herein, we compare GEM results with those available in literature. The first example concerns a flame propagation test over a problem domain, whose boundary conditions are as specified in Eq. (5). Ignition is initiated by exposing one of the walls to a dimensionless temperature of 0.6. When the wall temperature is so increased, the reactant is heated until ignition occurs, thereafter; the flame forms quickly and begins to propagate with an Arrhenius type reaction across the problem domain until the whole reactant is consumed.

Figs. 1 and 2 show temperature and mass profiles of the three models for a relatively low reaction rate $A = 2.2\times10^5$, a time step $\Delta t = 0.0002$ and activation energy $\theta = 4$. In order to allow for comparison with the work of Otey and Dwyer [17], fifty-one grid points are employed for this simulation, and corresponding points are plotted. A relatively close agreement between the models is observed with some deviations around the region of steep temperature gradients. The results were found to improve by placing more grids in the region of steep scalar gradients.

In order to further explore the physics of the problem, we decided to plot the mass fraction and temperature profiles to investigate what happens as time increases from $t = 0.005$ to $t = 0.015$. Figs. 3 and 4 show the results obtained with *model-1*. It is clear from this figures that the flame propagates from left to right as specified by the boundary conditions. This observation is further confirmed by the profiles of the scalar gradients for the temperature and shown in Fig. 5. It can be seen that the zones of combustion have been correctly identified for the time specified.

Fig. 6 shows the profiles of temperature and mass fraction as function of space at $t = 0.005$. The relatively steeper profiles of the field variables are likely to be a result of the higher reaction rate ($A = 1.98\times10^6$). When compared with Fig. 4 for the same time increment, the mass fraction approaches zero much earlier because of a higher combustion. This is in agreement with physics.

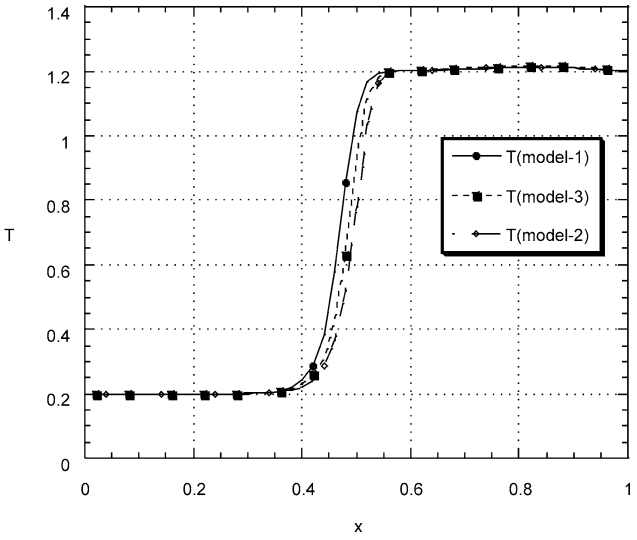

Fig. 1. Temperature profiles ($t = 0.015$).

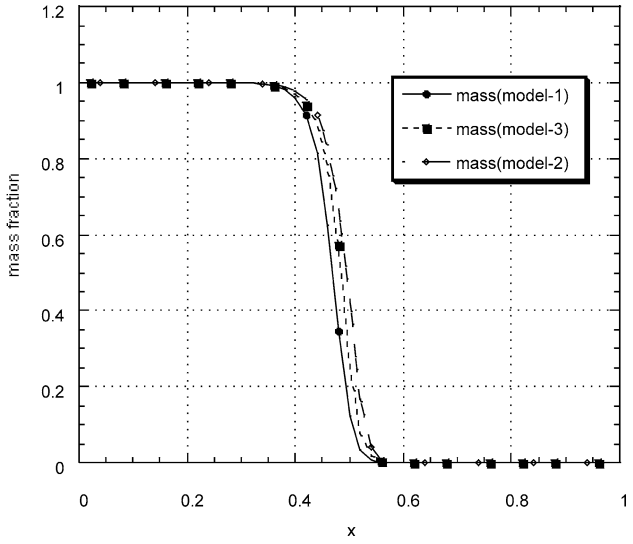

Fig. 2. Mass fraction profiles ($t = 0.015$).

Example 2. Our next task involves the determination of the rate of fuel depletion (Raizadeh 1979) and local Damköhler's number. A reaction rate $A = 1.98 \times 10^6$ is adopted for this test, and the boundary conditions remain as specified in Eq. (5). Fig. 7 shows the local Damköhler number as a function of distance at $t = 0.005$. Note that it is zero everywhere except at the reaction front. Fig. 8 illustrates the fuel depletion as a function of distance at $t = 0.015$. It has a zero value in the unburnt fuel region, and its value suddenly increases at the start of combustion until it attains a constant value. These observations serve to describe the physics of the problem.

Example 3. The ability of GEM to handle complex kinetics is demonstrated in this example. We investigate a rate term that represents a substrate inhibition kinetics like those found in enzyme catalyzed biochemical reaction. The problem is governed by Eq. (6).

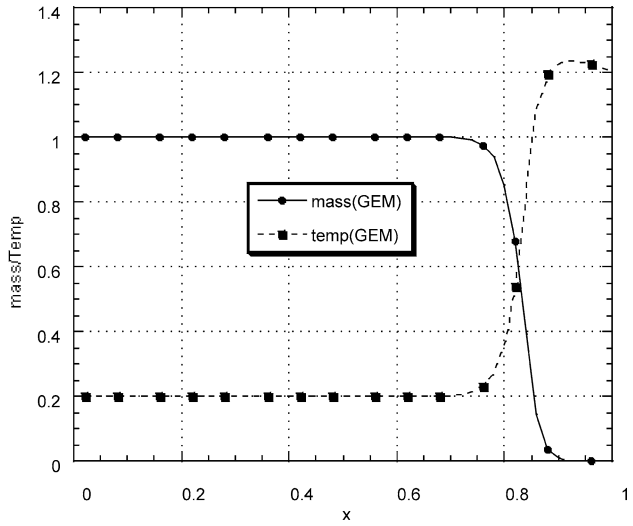

Fig. 3. Temperature and mass fraction profiles ($t = 0.005$).

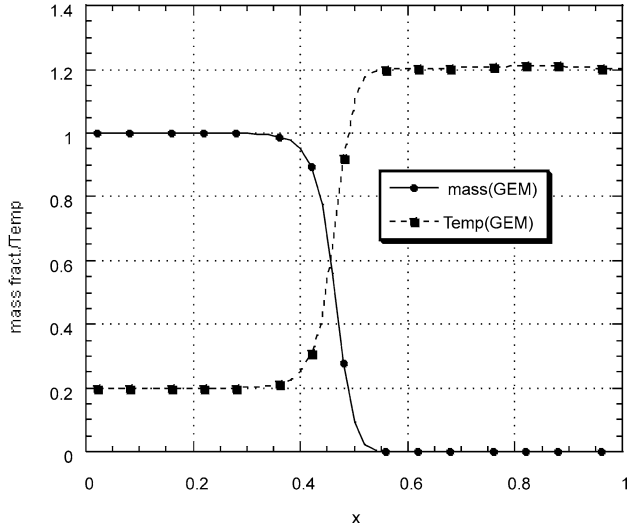

Fig. 4. Temperature and mass fraction profiles ($t = 0.015$).

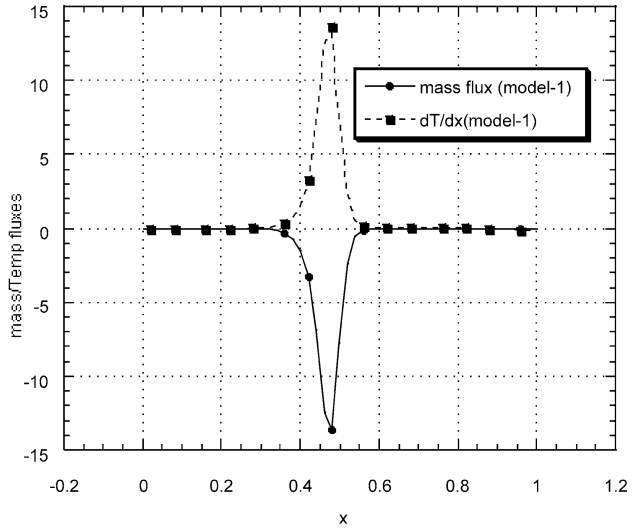

Fig. 5. Flux profiles ($t = 0.015$).

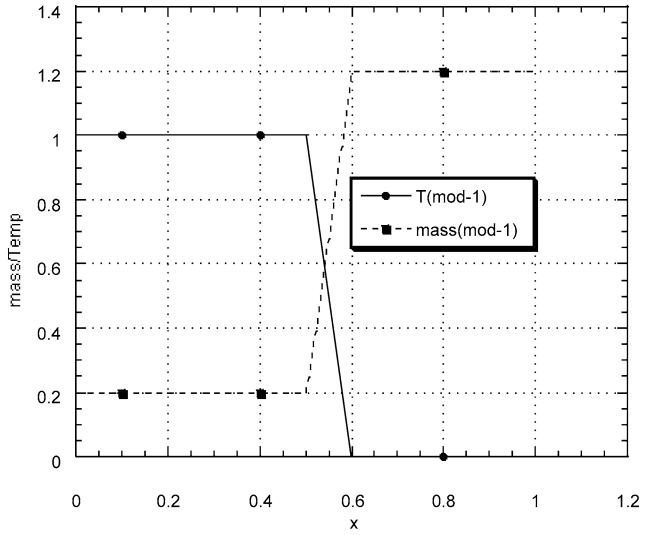

Fig. 6. Temperature and mass fraction profiles for higher reaction rate ($t = 0.005$).

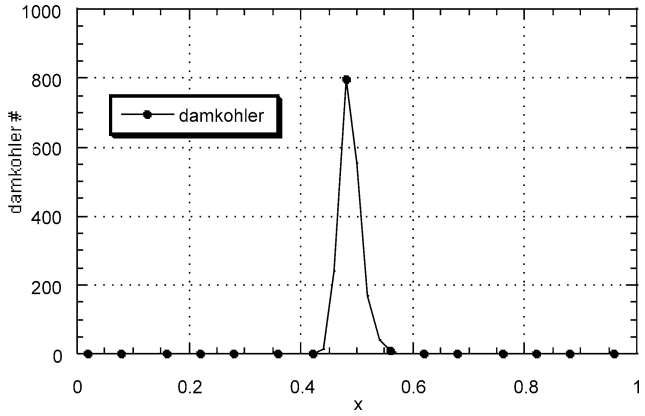

Fig. 7. Damkohler number profile ($t = 0.005$).

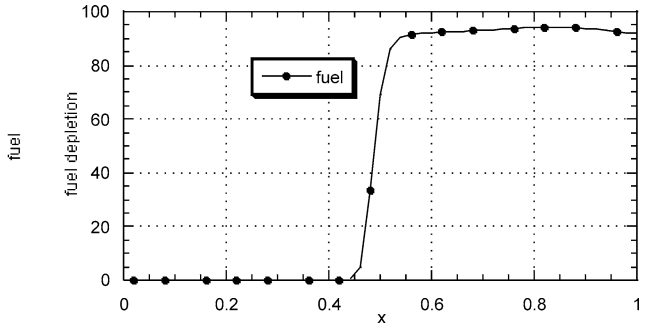

Fig. 8. Fuel depletion profile.

The rate form is nonlinear and depends on only on the concentration of the diffusing species. Linearization is accomplished by applying the Picard scheme (Eq. (13b)). This problem has been known to exhibit multiple solutions for certain ranges of M, c and β. While it is outside of the scope of this study to carry out a detailed investigation of the dynamics of chemically reacting systems that exhibit multiple solutions, however some of the results are worthy of some comments.

For this example, we consider slab geometry with a normalized domain of 0 to 1. The boundary specifications are a no flux condition at $x = 0$ and a unit concentration at $x = 1$. In order to compare GEM results with the boundary element method (BEM) results of Ramachandran [5], the following reaction parameters are chosen: $M = 100$, $c = 110$ and $\beta = 1000$, $D = 1.0$. It was found that the steady state solution was highly dependent on the starting concentrations (initial conditions). The problem was solved, by first of all imposing an initial concentration of unity at all the nodal points, and again with an initial concentration of zero. If two solutions are found to be the same, then only one solution exists, otherwise multiple solutions obtain. Table 1 shows a relatively close agreement between the GEM results obtained herein with the BEM results of Ramachandran [5]. Next, We carried out a sensivity analysis of the Thiele's modulus. The problem parameters c and β were kept constant while changing the value of the Thiele's modulus M. For each value of M, we tested two different initial conditions ($\phi(x, 0) = 0$ and $\phi(x, 0) = 1$) or starting values. Multiple solutions were found to exist in the following ranges of Thiele's modulus: $20.01 \leqslant \sqrt{M} \leqslant 26.95$. Outside of this range, only one solution was found to exist. This range of Thiels modulus was found to be close to Ramachandran [5] BEM solution. While it is obvious that multiplicity behavior is highly or solely dependent on the variability of certain problem parameters or initial conditions, an insight into the range of parameters where such activities are likely to occur could provide a guide to a reactor engineer as to how particular steady state may be achieved.

Example 4. To further validate GEM algorithm, we consider a case involving a cylindrical catalyst. The reaction term depends on both the dependent and space variables. This is known to arise from a deliberate design or mishap of catalyst poisoning. The second order reaction is described by:

Table 1
Multiple solution results

X	Reference [5]	GEM	Reference [5]	GEM
0.0	4.53e–03	4.48e–03	0.6702	0.6681
0.2	5.02e–02	4.98e–02	0.6843	0.6841
0.4	0.2073	0.2071	0.7259	0.7261
0.6	0.4349	0.4352	0.7937	0.8012
0.8	0.7035	0.7036	0.8858	0.8862
1.0	1.000	1.00	1.00	1.00
Ψ	1.563	1.558	0.622	0.623

Table 2
Results for a catalyst

Node Location	Reference [5]	GEM
0.0	0.6093	0.6104
0.4	0.6717	0.6720
0.7	0.8224	0.8227
0.75	0.8568	0.8574
0.85	0.9191	0.9187
1.0	1.0	1.0
Ψ	0.4979	0.4986

$$f(\varphi, x) = M\varphi^2, \quad x \leqslant 0.7$$

$$f(\varphi, x) = M\varphi^2 \mathrm{e}^{[-d(x-0.7)]}, \quad x \geqslant 0.7$$

The exponential term makes the reaction term to decay rapidly for values of x greater that 0.7. A cylindrical geometry is considered here, and the following problem parameters are used in this simulation: $M = 4$, $d = 1.0 \times 10^6$. This example is taken from Ramachandran [5]. The accuracy of the numerical results was verified by comparing GEM results obtained for 5 and 10 subintervals. Table 2 shows that they are relatively close.

5. Conclusion

We have applied GEM, a hybrid numerical solution technique based on BEM–FEM combination, to highly nonlinear diffusion–reaction problems involving different geometries, and to a combustion problem involving interactions between thermal and mass transfer processes. The models developed herein are based on integral replications of the governing partial differential equations along the lines of the boundary integral theory. By relying on the accuracy of the boundary element formulation, and the domain discretization of the boundary element method, GEM is able to handle nonlinear problems accurately and with minimum efforts. This work is a further attempt to apply boundary integral theory to problems that require domain discretization and complements attempts such as those of Samec and Skerget [19], Popov and Powers [10].

References

[1] G.A. Lavoie, J.B. Hewood, J.C. Beck, Experimental and theoretical study of nitric oxide formation in internal combustion engines, Combust. Sci. Technol. 1 (1970) 313–326.
[2] P.N. Blumberg, Nitric oxide emissions from stratified charge engines: Prediction and control, Combust. Technol. 8 (1973) 5–24.
[3] P.L. Mills, M.P. Dudukovic, P.A. Ramachandran, A numerical study of approximation methods of linear and nonlinear diffusion–reaction equation with discontinuous boundary conditions, Comput. Chem. Engrg. 12 (1988) 37–53.
[4] P.W. Patridge, L.C. Wrobel, Dual reciprocity boundary element method for spontaneous ignition, Internat. J. Numer. Methods Engrg. 30 (1990) 953–963.
[5] P.A. Ramachandran, Diffusion–Reaction problem revisited via a new boundary element discretization, Chem. Engrg. Sci. 45 (1990) 3525–3532.
[6] O.E. Lafe, J.A. Liggett, P.L.-F. Liu, Solutions of leaky, layered, confined, unconfined, nonisotropic aquifers, Water Res. Res. 17 (1981) 1431–1444.
[7] O.E. Lafe, A.H.D. Cheng, A perturbation boundary element code for steady state groundwater flow in heterogeneous aquifers, Water Res. Res. 23 (1987) 1079–1084.
[8] D. Nardini, C.A. Brebbia, A new approach in vibration analysis using boundary elements, Appl. Math. Modelling 7 (1983) 157–162.
[9] S. Ahmad, P.K. Banerjee, A new approach in vibration analysis by BEM using particular integrals, Internat. J. Numer. Methods Engrg. 113 (1986) 151–163.
[10] V. Popov, H. Powers, The DRM-MD integral equation method, Internat. J. Numer. Methods Engrg. 44 (1999) 327–353.
[11] R. Archer, R.N. Horne, O.O. Onyejekwe, Petroleum reservoir engineering applications for the dual reciprocity boundary element method and the Green element method, in: Advances in Boundary Element Method, WIT Press, Southampton, 1999, pp. 525–536.
[12] A.E. Taigbenu, The Green element method, Internat. J. Numer. Methods Engrg. 38 (1995) 2241–2263.
[13] A.E. Taigbenu, The Green Element Method, Kluwer Academic, Boston, USA, 1999.
[14] O.O. Onyejekwe, A Green element description of mass transfer in reacting systems, Numer. Heat Transfer 30 (1996) 483–498.
[15] O.O. Onyejekwe, A Green element treatment of isothermal flow with second order reaction, Internat. Comm. Heat Mass Transfer 97 (1997) 251–264.
[16] O.O. Onyejekwe, A boundary element—Finite element equation solutions to flow in heterogeneous porous media 31 (1998) 251–264.
[17] G.R. Otey, H.A. Dwyer, Numerical study of interaction of fast chemistry diffusion, AIAA J. 17 (1979) 603–613.
[18] F. Raizadeh, A study of reaction–diffusion problems with adaptive grids, M.S. Thesis, Department of Mech. Engineering, University of California at Davis, 1979.
[19] N. Samec, L. Skerget, Numerical modeling of premixed flames by boundary-domain integral method, 6th International Conference on Numerical Combustion, in: New Orleans, Lousiana, March 4–6, 1996.